Journal of Statistical Physics, Vol. 81, Nos. 3/4, 1995

Hierarchical Monte Carlo Methods for Fractal Random Fields

Frank W. Elliott, Jr.,[1] Andrew J. Majda,[1] David J. Horntrop,[1] and Richard M. McLaughlin[2]

Received January 19, 1995; final April 14, 1995

Two hierarchical Monte Carlo methods for the generation of self-similar fractal random fields are compared and contrasted. The first technique, successive random addition (SRA), is currently popular in the physics community. Despite the intuitive appeal of SRA, rigorous mathematical reasoning reveals that SRA cannot be consistent with any stationary power-law Gaussian random field for any Hurst exponent; furthermore, there is an inherent ratio of largest to smallest putative scaling constant necessarily exceeding a factor of 2 for a wide range of Hurst exponents H, with $0.30 < H < 0.85$. Thus, SRA is inconsistent with a stationary power-law fractal random field and would not be useful for problems that do not utilize additional spatial averaging of the velocity field. The second hierarchical method for fractal random fields has recently been introduced by two of the authors and relies on a suitable explicit multiwavelet expansion (MWE) with high-moment cancellation. This method is described briefly, including a demonstration that, unlike SRA, MWE is consistent with a stationary power-law random field over many decades of scaling and has low variance.

KEY WORDS: Fractal random fields; Monte Carlo methods; successive random addition.

1. INTRODUCTION

Generating random velocity fields which are fractal and self-similar over many scales by Monte Carlo methods that are accurate, efficient, and have

[1] Courant Institute of Mathematical Sciences, New York University, 251 Mercer Street, New York, New York 10012.
[2] Department of Mathematics, University of Utah, Salt Lake City, Utah 84112.

0022-4715/95/1100-0717$07.50/0

low variance is an important and challenging problem in diverse applications such as turbulent diffusion,[1-3] solute transport in groundwater,[4] turbulent combustion,[5] and random topography in statistical physics.[6] In the simplest context of a zero mean stationary scalar Gaussian random field $v(x)$ in a single space dimension, these fractal fields are completely characterized by the mean

$$\langle v(x) \rangle = 0$$

and the structure function

$$\langle [v(x) - v(y)]^2 \rangle = C_H |x - y|^{2H} \tag{1}$$

where $0 < H < 1$ is the Hurst exponent. Here and below for any random variable w, $\langle w \rangle$ denotes the expected value of w. The fact that the structure function in (1) grows with the distance between the points of evaluation is a manifestation of the strong long-range correlation of the field $v(\cdot)$ and this makes accurate and efficient Monte Carlo simulation of such fields a difficult task. The random field $v(\cdot)$ has the scaling property

$$v(x) = |\lambda|^{-H} v(\lambda x) \tag{2}$$

for any $\lambda \neq 0$, where here and below equality between random fields means that they share the same finite-dimensional distribution functions.

It is very natural to attempt to ensure both efficiency and scaling accuracy in a Monte Carlo simulation by approximating the fractal random field defined through (1) by an approximate random field $v_{\text{App}}(x)$ involving a hierarchy of scales, i.e.,

$$v_{\text{App}}(x) = \sum_{m=M_0}^{M_1} \tilde{v}_m(2^m x)\, 2^{-mH} \tag{3}$$

Here M_0 and M_1 are the largest and smallest scales and $\{\tilde{v}_m | m = 0, \pm 1, \pm 2, \ldots\}$ are independent identically distributed random fields which are localized in space for computational efficiency. In the idealized situation where truncation to a finite number of scales is ignored, i.e., $M_0 = -\infty$ and $M_1 = +\infty$, any approximate hierarchical method automatically satisfies the scaling property

$$\langle |v_{\text{App}}(x) - v_{\text{App}}(y)|^2 \rangle = 2^{-2H} \langle |v_{\text{App}}(2x) - v_{\text{App}}(2y)|^2 \rangle \tag{4}$$

which coincides for multiples of two with the scaling property in (1) for the fractal field $v(x)$. However, for a hierarchical method to be consistent with

the stationary fractal field $v(x)$ requires a much stronger condition. We define the quantity $D(x, y)$ by

$$D(x, y) = \langle |v_{\text{App}}(x) - v_{\text{App}}(y)|^2 \rangle \tag{5}$$

and $K(x, y)$ by

$$K(x, y) = D(x, y)\, |x - y|^{-2H} \tag{6}$$

In order for the hierarchical method from (3) to be consistent with the stationary fractal random field defined in (1) clearly $K(x, y)$ should be roughly constant and at least tend to a constant as the finite truncation parameters M_0, M_1 from (3) become infinite.

One intuitively appealing Monte Carlo method for generating fractal random fields that is currently popular in the physics community is the method of successive random addition (SRA) introduced by Voss.[6, 7] Recently, Viecelli and Canfield[8] have recommended using SRA for the simulation of stationary turbulent incompressible velocity fields. Section 2 contains the main new results presented here. First, we show that SRA can be recast as a hierarchical method with the structure in (3). Then, we demonstrate with rigorous mathematical bounds that SRA cannot be consistent with the stationary Gaussian random field defined in (1) both for the idealized case of an infinite number of scales as well as the practical case with a finite number of scales. In both the finite and infinite situations, we show that the ratio of the maximum to the minimum value of $K(x, y)$ from (6) necessarily exceeds 1 for all Hurst exponents H with $0 < H < 1$ and definitely exceeds 2 for all Hurst exponents H, with of $0.30 < H < 0.85$. Thus, despite the scaling property in (4) and its intuitive attractiveness, SRA is inconsistent with a stationary fractal random field with necessarily large scatter in the values for $K(x, y)$. In particular, this large range of values of $K(x, y)$ makes SRA inappropriate for use in situations such as calculating turbulent diffusion where preserving stationarity is necessary because accurate values of a stationary velocity field are needed to validate preconstants for scaling laws for quantities such as pair dispersion.[8–10] For physical applications in which additional spatial averaging of the velocity field can be utilized, this scatter in the value of $K(x, y)$ may not be so catastrophic.

A second hierarchical method involving a suitable explicit multiwavelet expansion (MWE) with high-moment cancellation has been developed quite recently by two of the authors[9–11] and applied to turbulent diffusion with random fractal velocity fields. In Section 3, we briefly describe this method and demonstrate both the consistency of this algorithm in generating approximations to the fractal random field $v(x)$ defined through (1) as well as the low variance of the method when finite sample sizes are included.

For example, with the value of the Hurst exponent $H = 1/3$, which corresponds to the Kolmogorov Spectrum, 12 decades of the correct scaling behavior in (1) with the constant prefactor accurate to 6% are generated with only 100 realizations and in an economical fashion so that less than 2000 active computational elements are needed in each realization. Furthermore, through random plane waves, the MWE method generalizes readily to higher dimensions with similar (spectacular) computational capabilities regarding both the velocity structure function[10] and pair dispersion in turbulent diffusion.[11] We refer the interested reader to ref. 9 for a detailed description and validation of the wavelet Monte Carlo method in a single space dimension and to refs. 10 and 11 for a detailed description of the multidimensional algorithm as well as applications in turbulent diffusion.

2. SUCCESSIVE RANDOM ADDITION AS A HIERARCHICAL METHOD

We begin by formulating the SRA algorithm from refs. 6 and 7 as a hierarchical method as described in (3) above. Successive random addition constructs a field by dyadic expansion. By definition, a dyadic rational number x satisfies $x = 2^{-m}n$ for some integers m and n, the *octave* and the *translate*, respectively. For each octave m, successive random addition constructs a piecewise linear field $v_m(\cdot)$. First, the method assigns an independent standard Gaussian random variable as the value of the field $v_m(x)$ at $x = n$ for $n = 0, \pm 1, \pm 2, \ldots$. Next, the method extends $v_m(\cdot)$ to all other points by linear interpolation. Finally, it scales $v_m(\cdot)$ to $2^{-mH} v_m(2^m \cdot)$ and sums from $m = M_0$ to $m = M_1$ to produce the field $v_{\text{App}}(\cdot)$ determined by the equations

$$\begin{aligned} \tilde{v}(x) &= g(\lfloor x \rfloor)(1 - [x]) + g(\lfloor x \rfloor + 1)[x] \\ v_{\text{App}}(x) &= \sum_{m=M_0}^{M_1} \tilde{v}_m(2^m x) 2^{-mH} \end{aligned} \tag{7}$$

Here $\lfloor x \rfloor$ is the greatest integer less than x, $[x] = x - \lfloor x \rfloor$ is the fractional part of x, while $\{ g(n) \mid n = 0, \pm 1, \pm 2, \ldots \}$ is a set of independent and identically distributed Gaussian random variables and $\{ \tilde{v}_m(\cdot) \mid m = 0, \pm 1, \pm 2, \ldots \}$ is a set of independent realizations of $\tilde{v}(\cdot)$. The structure function of the successive random addition field is defined in terms of the structure functions for the piecewise linear fields as follows:

$$\begin{aligned} D(x, y) &= \langle [v_{\text{App}}(x) - v_{\text{App}}(y)]^2 \rangle \\ &= \sum_{m=M_0}^{M_1} \tilde{D}(2^m x, 2^m y) 2^{-2mH} \end{aligned} \tag{8}$$

with

$$\tilde{D}(x, y) = \langle [\tilde{v}(x) - \tilde{v}(y)]^2 \rangle$$

Of course, the structure function of the field $\tilde{v}(\cdot)$ is somewhat complicated. We calculate explicitly that for SRA $\tilde{D}(x, y)$ is given by

$$\tilde{D}(x, y) = \begin{cases} 2(x-y)^2 & \text{if } \lfloor x \rfloor - \lfloor y \rfloor = 0 \\ (1-[x])^2 + ([x]-1+[y])^2 + [y]^2 & \text{if } \lfloor y \rfloor - \lfloor x \rfloor = 1 \\ (1-[y])^2 + ([y]-1+[x])^2 + [x]^2 & \text{if } \lfloor x \rfloor - \lfloor y \rfloor = 1 \\ (1-[x])^2 + [x]^2 + (1-[y])^2 + [y]^2 & \text{if } |\lfloor x \rfloor - \lfloor y \rfloor| > 1 \end{cases} \tag{9}$$

where $[x] = x - \lfloor x \rfloor$.

2.1. Inconsistency of SRA with Infinitely Many Scales

For simplicity in exposition, we first consider SRA defined in (7) in the idealized case where $M_0 = -\infty$ and $M_1 = +\infty$ so that there are an infinite number of octaves present. In this case our first argument for the inconsistency of SRA is elementary and straightforward, but also serves as a prototype for the more complex reasoning needed for the case with finitely many octaves developed in the next subsection.

To demonstrate the inconsistency of SRA, we need to show that the function $K(x, y)$ defined in (6) is not a constant. We define an infinite sequence of pairs of points (x_p, y_p) for $p = 1, 2, 3, \ldots$ given by

$$x_p = \tfrac{1}{2} - 2^{-p}, \qquad y_p = \tfrac{1}{2} + 2^{-p} \tag{10}$$

We explicitly calculate the numbers $K(x_p, y_p) = K_p$ utilizing the formulas in (8) and (9) with $M_0 = -\infty$ and $M_1 = +\infty$ to obtain

$$\begin{aligned} K_p = {} & 2 \cdot 2^{2(1-p)(1-H)} \sum_{m=-\infty}^{0} 2^{2m(1-H)} \\ & + \tfrac{1}{2} \cdot 2^{2(1-p)(1-H)} \sum_{m=1}^{p-1} 2^{2m(1-H)} \\ & + 2 \cdot 2^{2(p-1)H} \sum_{m=p-1}^{\infty} 2^{-2mH} \end{aligned} \tag{11}$$

The interested reader can check that this sequence is monotone decreasing with

$$K_1 = 2[1 + (4^{(1-H)} - 1)^{-1}] + 2(4^H - 1)^{-1} \tag{12}$$

and the limit as p tends to infinity K_∞ given by

$$K_\infty = \tfrac{1}{2}[1 + (4^{(1-H)} - 1)^{-1}] + 2(4^H - 1)^{-1} \tag{13}$$

For a Hurst exponent H with $0 < H < 1$ we trivially have $K_1 > K_\infty$ and the ratio K_1/K_∞ as a function of H is graphed in Fig. 1; the inequality $K_1 > K_\infty$ rigorously guarantees that SRA with infinitely many scales is not consistent with a stationary power-law random field as defined in (1) above. By a calculation similar to the one in Eq. (11), it can be shown that $K(x_p, 1/2) = K_1$ for all p. A comparison of this result with the result in (13) demonstrates that the function $K(x, y)$ has a discontinuity of at least $\frac{3}{2}[1 + (4^{(1-H)} - 1)^{-1}]$ at (1/2, 1/2); indeed, by scaling it can be shown that the same discontinuity occurs at *every* dyadic rational number on the diagonal. The presence of these large, dense (and, hence, unavoidable) discontinuities in K further indicates the inconsistency of SRA.

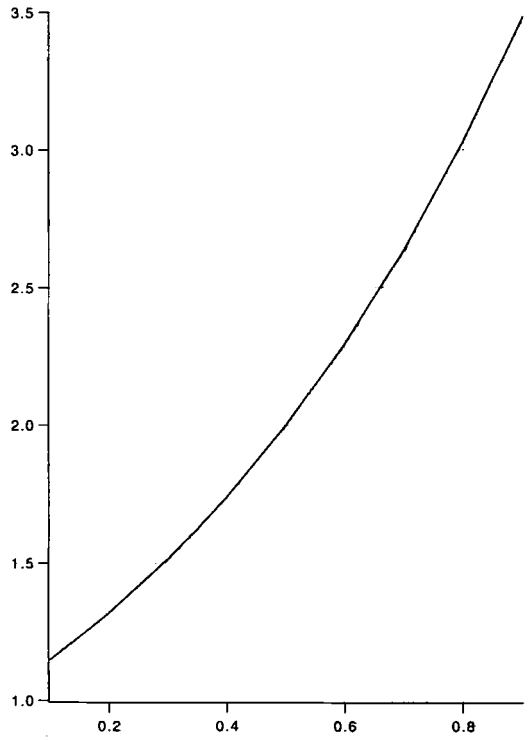

Fig. 1. The ratio of K_1 to K_∞ versus the Hurst exponent H.

Nevertheless, it is possible to show that the inconsistency of SRA is, at least, bounded. With further tedious calculations we can establish that

$$K_1 = M = \max_{(x,y)\in R^2} K(x,y)$$

and also that (14)

$$0 < L = \min_{(x,y)\in R^2} K(x,y)$$

is finite for this idealized situation for SRA with infinitely many scales; clearly, we have $L \leqslant K_\infty < K_1 = M$ as bounds. We omit the cumbersome proof of the facts claimed in (14) since they are not essential for the main results presented in this paper.

2.2. Inconsistency of SRA with Finitely Many Scales

One criticism of the argument just presented in Section 2.1 is the fact that it relies on the use of an infinite number of scales in SRA, so that perhaps the bounds for inconsistency utilizing K_1 and K_∞ are unduly pessimistic when M_0 and M_1 in (7) are finite. Here, through more sophisticated but similar arguments, we establish that quantitatively similar bounds are valid and imply the inconsistency of SRA with finitely many scales.

To avoid spurious effects with very small numbers of octaves in the sum in (7), we fix a minimum number of octaves $L+1$ and consider SRA with finitely many scales so that in (7)

$$M_0 = -p, \qquad M_1 = L + q, \qquad p, q \geqslant 0 \tag{15}$$

The reader can think of L as some small fixed number of octaves, i.e., L satisfies $5 \leqslant L \leqslant 10$. Our strategy will be to vary p and q with $p, q \geqslant 0$ so that we minimize the range of the function $K(x,y)$ defined in (6); thus, we attempt to find the SRA algorithm with finitely many scales which is the "best candidate" to be consistent with the stationary fractal random field characterized by (1). For a given p and q we denote by $K_{pq}(x,y)$ the function defined in (6) by the finite truncation of SRA described in (7) and (15).

As in Section 2.1, to investigate the range of $K_{pq}(x,y)$ we restrict our attention to the value of this function on a finite collection of points. In particular we consider only x and y, which are distinct points in the unit

interval and which are integer multiples of 2^{-L}. This assumption greatly simplifies the application of formulas (8) and (9), giving

$$\begin{aligned} D(x, y) &= \sum_{m=-p}^{L+q} \tilde{D}(2^m x, 2^m y)\, 2^{-2mH} \\ &= \sum_{m=-p}^{-1} \tilde{D}(x, y)\, 2^{2m(1-H)} + \sum_{m=L+1}^{L+q} \tilde{D}(2^L x, 2^L y)\, 2^{-2mH} \\ &\quad + \sum_{m=0}^{L} \tilde{D}(2^m x, 2^m y)\, 2^{-2mH} \end{aligned} \tag{16}$$

In the preceding equation, the summation over $m<0$ becomes a geometric series because $\|\lfloor 2^m x \rfloor - \lfloor 2^m y \rfloor\| = 0$, so that $\tilde{D}(2^m x, 2^m y) = 2(2^m x - 2^m y)^2$ according to formula (9). Also, the summation over $m>L$ becomes a geometric series because $2^m x$ and $2^m y$ are integers which differ in magnitude by at least 2, so that $\tilde{D}(2^m x, 2^m y) = 2$ according to formula (9). Because these two terms are geometric series, we can evaluate $K_{pq}(x, y)$ even when p or q is infinite. We further restrict our attention to $(x, y) \in \{[0, 1/2) \times [1/2, 1)\}$, so we are left with

$$S_L = \{[0, \tfrac{1}{2}) \times [\tfrac{1}{2}, 1)\} \cap \{\mathbf{Z} 2^{-L}\}^2 \tag{17}$$

i.e., the set of points in $[0, 1/2) \times [1/2, 1)$ which have coordinates which are integer multiples of 2^{-L}. We will now show that the range of the function $K_{pq}(x, y)$ on S_L is unacceptably large by finding a rigorous lower bound Q' for this range.

If we define

$$K_{pq}^{\max} = \sup_{(x, y) \in S_L} K_{pq}(x, y) \tag{18a}$$

$$K_{pq}^{\min} = \inf_{(x, y) \in S_L} K_{pq}(x, y) \tag{18b}$$

then we seek a lower bound on the ratio of $K_{pq}^{\max}$ to $K_{pq}^{\min}$ as p and q vary. According to formula (16), $K_{pq}(x, y)$ is increasing and convergent in p and q. Therefore, $K_{pq}^{\max}$ and $K_{pq}^{\min}$ are both increasing and convergent in p and q. This fact facilitates a rigorous estimate of the minimum of the desired ratio by reducing an infinite minimization problem to a finite minimization

problem. We begin by dividing the problem of estimating the minimum of the ratio into four parts,

$$Q = \inf_{p,\, q \geqslant 0} \frac{K_{pq}^{\max}}{K_{pq}^{\min}} \tag{19a}$$

$$Q = Q_1 \wedge Q_2 \wedge Q_3 \wedge Q_4 \tag{19b}$$

$$Q_1 = \min_{0 \leqslant p,\, q \leqslant n} \frac{K_{pq}^{\max}}{K_{pq}^{\min}} \tag{19c}$$

$$Q_2 = \min_{0 \leqslant p \leqslant n} \inf_{n \leqslant q} \frac{K_{pq}^{\max}}{K_{pq}^{\min}} \tag{19d}$$

$$Q_3 = \min_{0 \leqslant q \leqslant n} \inf_{n \leqslant p} \frac{K_{pq}^{\max}}{K_{pq}^{\min}} \tag{19e}$$

$$Q_4 = \inf_{n \leqslant p,\, q} \frac{K_{pq}^{\max}}{K_{pq}^{\min}} \tag{19f}$$

Here $a \wedge b$ is the minimum of a and b. Term Q_1 involves a finite search, but the other three terms involve minimization over an infinite set. Therefore, we use the monotonicity of $K_{pq}^{\max}$ and $K_{pq}^{\min}$ to obtain a lower bound on the ratio involving a finite set of cases. Thus, we have

$$Q \geqslant Q'$$

$$Q' = Q_1 \wedge Q_2' \wedge Q_3' \wedge Q_4'$$

$$Q_1 = \min_{0 \leqslant p,\, q \leqslant n} \frac{K_{pq}^{\max}}{K_{pq}^{\min}} \tag{20a}$$

$$Q_2' = \min_{0 \leqslant p \leqslant n} \frac{K_{pn}^{\max}}{K_{p\infty}^{\min}} \tag{20b}$$

$$Q_3' = \min_{0 \leqslant q \leqslant n} \frac{K_{nq}^{\max}}{K_{\infty q}^{\min}} \tag{20c}$$

$$Q_4' = \frac{K_{nn}^{\max}}{K_{\infty\infty}^{\min}} \tag{20d}$$

Below we will choose an n large enough so that $K_{pn}^{\max}$, $K_{nq}^{\max}$, and $K_{nn}^{\max}$ are near their limiting values for $0 \leqslant p,\, q \leqslant n$.

The comparison problem in (20) for the ratio Q' can be evaluated numerically for a fixed H and L in a straightforward fashion by utilizing

Table I. Effect of Varying p and q on $K_{pq}^{\max}/K_{pq}^{\min}$ for $H=1/3$, $L=8$, and $n=10$

p	$q=0$	$q=1$	$q=2$	$q=10$	$q=\infty$
0	3.014	3.072	3.109	3.147	3.147
1	2.251	2.270	2.284	2.311	2.311
2	2.188	2.183	2.190	2.206	2.206
10	2.173	2.126	2.108	2.106	2.106
∞	2.177	2.128	2.109	2.104	2.104

(16), since Q' involves a search through only a finite number of cases, yet provides a rigorous lower bound on the ratio. We illustrate the results of this procedure for the Hurst exponent $H=1/3$, $L=8$, and $n=10$. Table I gives the ratio of $K_{pq}^{\max}$ to $K_{pq}^{\min}$. In this table, p is the row number and q is the column number, while the dots indicate an omitted range of indices.

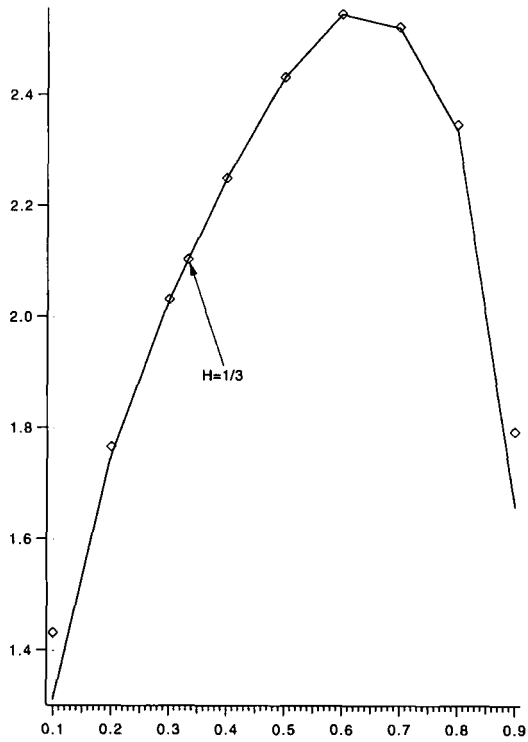

Fig. 2. The quantities Q' (solid line) and $K_{\infty\infty}^{\max}/K_{\infty\infty}^{\min}$ (diamonds) versus the Hurst exponent H.

We observe that no ratio is ever smaller than 2.1, so that SRA with finitely many scales is inconsistent with a stationary fractal random field and necessarily has large fluctuations in the prefactor exceeding 2.1 in size.

The ratio $K_{\infty\infty}^{\max}/K_{\infty\infty}^{\min}$ denotes the range of $K(x, y)$ over the set S_L defined in (17) with infinitely many scales. The finite set S_L differs from the infinite set used in Section 2.1, so that the resulting estimate of the ratio is different. We used the numerical procedure from the previous paragraph to calculate Q' from (20) for the values $H = 0.1, 0.2, 0.3, \ldots, 0.9$ and $H = 1/3$; we also calculated $K_{\infty\infty}^{\max}$ with $L = 8$. In Fig. 2, the solid line is the graph of Q' through these points, while the ratio $K_{\infty\infty}^{\max}/K_{\infty\infty}^{\min}$ is depicted by diamonds. The lower bound extracted from Q' in Fig. 2 indicates that SRA with a finite number of scales is inconsistent with a ratio exceeding 1.8 for most H in $(0, 1)$. Finally, the close agreement between the line plot and the diamond plot in Fig. 2 indicates that the use of a finite number of truncated scales in SRA does not improve appreciably the inherent inconsistency of SRA with an infinite number of scales as demonstrated earlier in Section 2.1.

We emphasize that Q' is a lower bound for fluctuations in SRA, so that even the results reported here might be optimistic. For a fixed H and L, there are no parameters other than p and q which can be adjusted in an SRA simulation, so that any use of SRA for generating stationary fractal fields must inherently involve the large errors documented here.

2.3. Histograms for the Coefficient Distribution in SRA

One conceivable objection to the analysis presented in Sections 2.1 and 2.2 is that those are extreme cases and for "most values of (x, y)" the function $K(x, y)$ defined in (6) is "nearly constant." Here we demonstrate that the above scenario is not valid, by calculating histograms for the coefficient distribution in SRA. For simplicity in exposition, we consider SRA with an infinite number of scales in (7), i.e., $M_0 = -\infty$ and $M_1 = +\infty$. When there are an infinite number of scales, it is a simple exercise to deduce that the distribution of values of the coefficient $K(x, y)$ over the region

$$S = \{(x, y) \mid 0 \leqslant x < 1 \leqslant y < 2\}$$

is sufficient to defermine the complete distribution of values over R^2.

With M defined in (14), in Fig. 3 we present a histogram of the values of the normalized function $K(x, y)/M$ on the unit square S with a 32×32 discretization and for the Hurst exponents $H = 0.2$, 0.4, 0.6, and 0.8. The area under the histogram between two points v_1 and v_2 reflects the area of

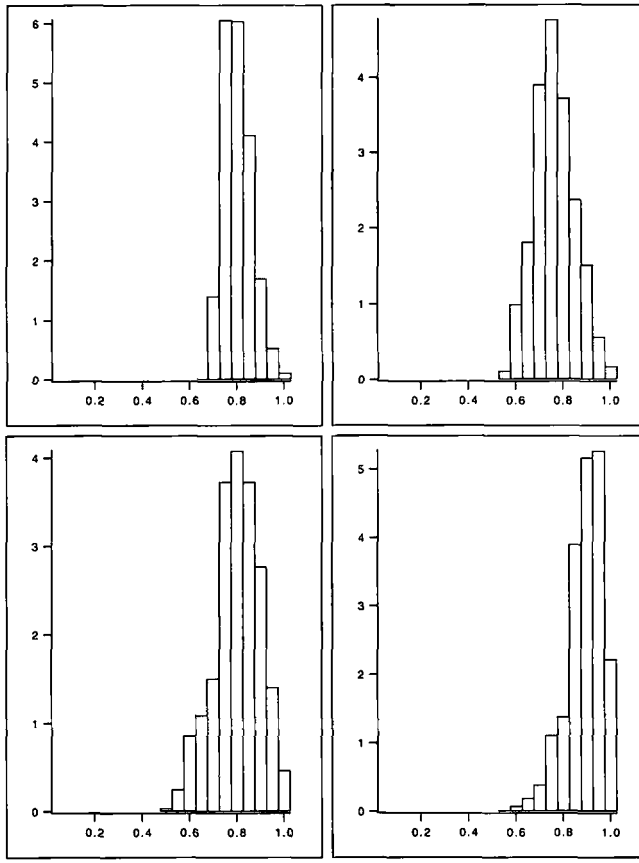

Fig. 3. Coefficient $K(x, y)$ distributions for SRA with (A) $H = 0.2$, (B) $H = 0.4$, (C) $H = 0.6$, and (D) $H = 0.8$.

S for which $v_1 \leqslant K(x, y)/M \leqslant v_2$. For each of these four cases, the distribution of the coefficient values is rather broad and does not lie in a narrow range. Furthermore, nothing can be done with SRA to reduce this range.

3. HIERARCHICAL METHODS BASED ON MULTIWAVELET EXPANSION

First, we briefly summarize some of the main steps in designing these hierarchical methods and refer the interested reader to ref. 9 for complete details regarding the implementation. The starting point for designing these methods is the representation of the random fractal velocity field $v(\cdot)$

characterized through (1) as a stochastic integral given by a moving average with respect to white noise,[9] i.e.,

$$v(x) = \int |x-y|^{H-1/2}\, dW(y) \tag{21}$$

where $dW(y)$ is Gaussian white noise. The second step is an exact result involving expansion of white noise by a general L^2-orthonormal basis, i.e., if $\{\psi_k(y)\}_{k=1}^{\infty}$ is a complete orthonormal basis for $L^2(R)$, then

$$dW(y) = \sum_k \psi_k(y)\, N_k \tag{22}$$

where N_k are standard independent identically distributed Gaussian random variables with mean zero and variance one. Inserting (22) into (21), we obtain the identity

$$v(x) = \sum_k N_k \int |x-y|^{H-1/2}\, \psi_k(y)\, dy \tag{23}$$

To obtain a general hierarchical method which yields an exact representation of $v(x)$, we choose the orthonormal basis in the hierarchical form[9]

$$\psi_k(y) = \phi_{mn}^{\sigma\tau} = 2^{m/2} \phi^{\sigma\tau}(2^m y - n) \tag{24}$$

where m and n are arbitrary integers and $\{\phi^{\sigma\tau}(y)\}_{\sigma=1}^{\tau}$ is a fixed finite set of functions. By inserting the functions in (24) into (23), we obtain the general exact hierarchical expansion[9]

$$v(x) = \sum_{m=-\infty}^{\infty} \tilde{v}_m(2^m x)\, 2^{-mH} \tag{25}$$

with

$$\tilde{v}_m(x) = \sum_{n=-\infty}^{\infty} \sum_{\sigma=1}^{\tau} G^{\sigma\tau}(x-n)\, N_{mn}^{\sigma\tau} \tag{26}$$

and $\{G^{\sigma\tau}(x)\}$ is the finite family of explicit functions given by

$$G^{\sigma\tau}(x) = \int_{-\infty}^{\infty} |x-y|^{H-1/2}\, \phi^{\sigma\tau}(y)\, dy \tag{27}$$

for $\sigma = 1,\ldots, \tau$. The representation of the stationary fractal random field $v(x)$ through the hierarchical method described in (25)–(27) is exact for any

choice of a complete orthonormal basis for $L^2(R)$ defined through $\{\phi_{mn}^{\sigma\tau}\}$ from (24). In particular, in the limit of an infinite number of scales, unlike the SRA algorithm discussed in Section 2, these hierarchical methods in (25)–(27) are always stationary, so that $K(x, y)$ in (6) is identically constant.

On the other hand, one of the intuitively appealing features of the SRA algorithm described in (7) and (8) is that it is extremely localized through linear interpolation, so that there is the possibility of great computational efficiency. In order to convert the hierarchical expansion in (25)–(27) into a practical efficient numerical method, it is obviously important to pick functions $\{\phi^{\sigma\tau}(y)\}_{\sigma=1}^{\tau}$ to localize the convolutions $G^{\sigma\tau}(x)$ in (27) while still having $\{\phi_{mn}^{\sigma\tau}\}$ from (24) generate a complete orthonormal basis for $L^2(R)$. The way to achieve this is developed in detail in ref. 9, where the Alpert–Rokhlin multiwavelet basis is utilized. The Alpert–Rokhlin multiwavelet[12]

$$\{\phi^{\sigma\tau} \mid \sigma = 1, 2, \ldots, \tau\}$$

is a set of τ functions which are supported on the interval $[0, 1]$, are piecewise polynomial on $[0, 1/2]$ and on $[1/2, 1]$, and satisfy the moment cancellation conditions

$$\int_{-\infty}^{\infty} x^p \phi^{\sigma\tau}(x)\, dx = 0, \qquad p = 0, 1, \ldots, \tau - 1 \tag{28}$$

In addition, the set of functions $\{\phi_{mn}^{\sigma\tau}\}$ defined in (24) by translation and scaling are a complete orthonormal basis for $L^2(R)$. A concise summary of the Alpert–Rokhlin wavelets including explicit formulas is presented in ref. 9. Clearly, the moment cancellation property in (28) for a large enough value of τ guarantees that $G^{\sigma\tau}(x)$ from (27) is highly localized so that the sum over the translates n in (26) for a fixed octave m converges rapidly.[9] In practice, the value $\tau = 4$ is sufficient for accurate simulation for the Hurst exponent $H = 1/3$ corresponding to the Kolmogorov spectrum.[9–11] In practice, we limit the algorithm in (25)–(27) to a finite number of scales M and we limit the translates $\phi_{mn}^{\sigma\tau}$ to those with support within a fixed distance b from x through rigorous energy criteria.[9] Through these judicious choices, properties such as stationarity of the field are very nearly preserved. The resulting hierarchical algorithm is given by

$$v(x) = \sum_{m=0}^{M-1} \tilde{v}_m^b(2^m x)\, 2^{-mH} \tag{29}$$

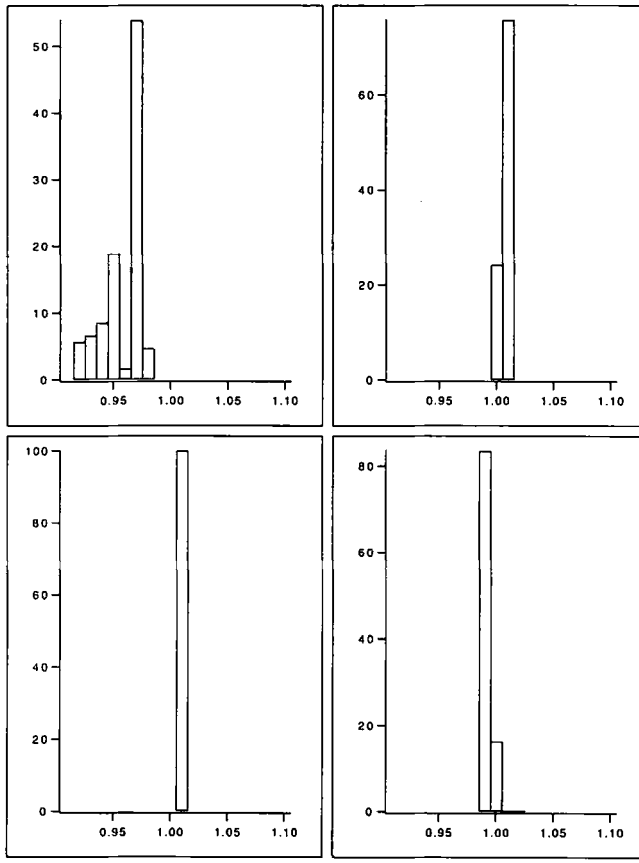

Fig. 4. Coefficient $K(x, y)$ distributions for MWE with (A) $H = 0.2$, (B) $H = 0.4$, (C) $H = 0.6$, and (D) $H = 0.8$. In all cases $\tau = 8$, $b = 15$, and the number of scales is 40.

with

$$\tilde{v}_m^b(x) = \sum_{\sigma=1}^{\tau} \sum_{n=\lfloor x \rfloor - b}^{\lfloor x \rfloor + b} G^{\sigma\tau}(x-n)\, N_{mn}^{\sigma\tau} \tag{30}$$

(The actual algorithm implemented below involves the use of Legendre polynomials at the largest scale, $m = 0$, but this modification is irrelevant for our treatment here.[13])

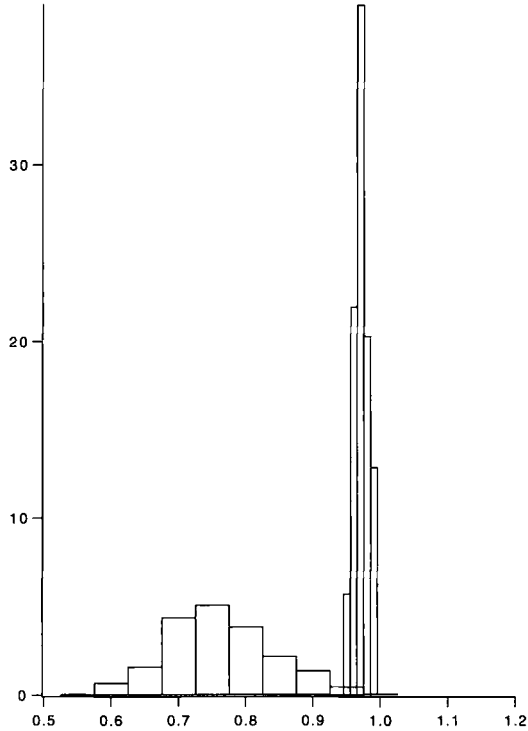

Fig. 5. Coefficient $K(x, y)$ distributions with $H = 1/3$ (Kolmogorov) for SRA (left) and MWE (right). For MWE, $\tau = 4$, $b = 5$, and the number of scales is 40.

3.1. Numerical Results for the MWE Method

In Figure 4 we show the histograms for Hurst exponents $H = 0.2$, 0.4, 0.6, and 0.8 for the range of the constant $K(x, y)$ in (6) computed through the finite-scale, wavelet band-limited, hierarchical algorithm defined in (29) and (30) with $M = 40$ scales, a wavelet order $\tau = 8$, and bandwidth $b = 15$. The histograms are computed in the same fashion as described in Section 2.3 for SRA. As in Section 2.3, these histograms are computed without the effects of sampling errors in the Gaussian random variables and without spatial averaging for any sort. The histograms for $H = 0.4$, 0.6, 0.8 all are highly localized and confined to a very narrow width with only a few percent variation. The histogram for the case $H = 0.2$ is somewhat broader, but is still confined to a much narrower region when compared to any of

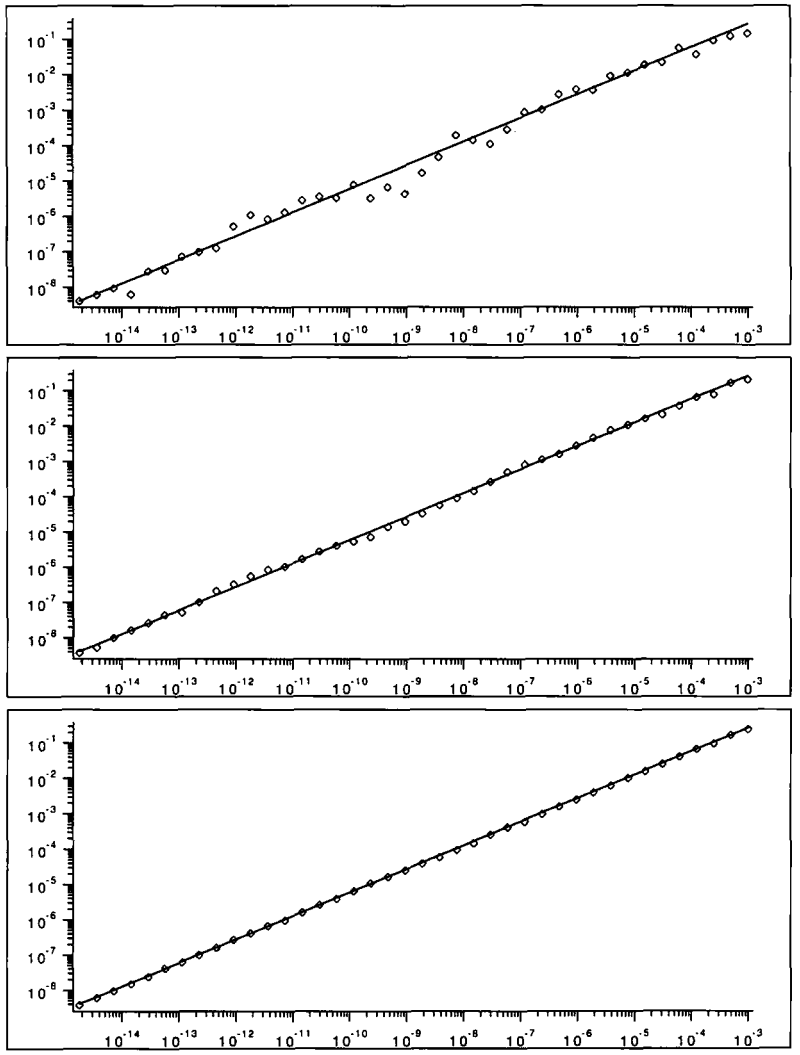

Fig. 6. Structure function with $H = 1/3$ for Monte Carlo-simulated MWE field with (A) 10, (B) 100, and (C) 1000 realizations. Each simulated value is plotted with a diamond; the true expected value is plotted with a solid line.

the cases of SRA presented earlier in Fig. 3. For direct comparison, in Fig. 5 we present two different histograms for the range of $K(x, y)$ for the Hurst exponent $H = 1/3$ corresponding to the Kolmogorov value. For the MWE method we used $M = 40$ scales, the wavelet order $\tau = 4$, and the bandwidth $b = 5$, while we compared this with the histogram for SRA with infinitely many scales. The histogram with the narrow spike in coefficient distribution corresponds to MWE, while the broad band histogram for the coefficient distribution in Fig. 5 is generated by the SRA algorithm.

The parameters for the MWE method with $M = 40$, $\tau = 4$, and $b = 5$ are essentially those utilized in refs. 10 and 11 for the generation of fractal fields in two space dimensions with many decades of scaling[10] and for turbulent diffusion with fractal velocity fields.[11] Finally, here we demonstrate the small stochastic errors and low variance with the MWE algorithm with these practical parameters in the simpler context of a single space dimension. We present the numerically computed structure function from (1) via the MWE algorithm with the above parameters for a finite sample size with 10, 100, and 1000 realizations, respectively, in Figs. 6A–C. For all three sample sizes, including the one with 10 realizations, the power law fit is 0.66 over 12 decades of scaling. Furthermore, in the last case with 1000 realizations, the constant prefactor is accurate to less than 8% over the entire 12 decades of scaling. Nevertheless, less than 2500 active computational elements are needed to generate each realization. The interested reader might want to compare further the results in ref. 10 for MWE in two dimensions with those via SRA described in ref. 8.

4. CONCLUDING REMARKS

It is worthwhile to briefly mention some other recent work on the generation of self-similar random fields in order to put the authors' current work in proper perspective. This will be followed by a summary of the results presented here. The method proposed by Eggers and Grossman is based upon a hierarchical-like superposition of eddies.[14] However, this technique does not preserve stationarity without spatial averaging,[14] making it inappropriate for the statistical issues considered here, which are geared toward high numerical accuracy with low variance for the velocity field for use in validating fundamental constants in turbulent diffusion, pair dispersion, etc. In Juneja *et al.*[15] a family of schemes is introduced that are modifications of an SRA-like approach. The goal of this family of schemes is to simulate more turbulence-like fields that have increments with nonzero skewness and that include small-scale intermittency.[15] Attempts to introduce such features in a simulated field are certainty interesting and

important, but, as noted earlier, are not the goal of our current work. Benzi *et al.* propose the use of wavelets to generate random fields.[16] The choice of wavelets in ref. 16, the Mexican hat function, suffers from many problems when compared with the Alpert–Rokhlin multiwavelets used here and in refs. 9–11. The Mexican hat function is not compactly supported, does not cancel many moments, and does not allow the convolutions $G^{\sigma\tau}$ to be computed exactly. As was demonstrated explicitly and described in detail in ref. 9, these features are all of utmost importance in designing an efficient and accurate wavelet-based approach to simulation for random velocity fields with a range of statistical scales spanning many decades.

We have compared and contrasted two very different but attractive hierarchical methods for the simulation of fractal random fields, SRA and MWE. In Section 2, we have given conclusive and mathematically rigorous evidence that despite its intuitive appeal, the SRA algorithm cannot be consistent with any stationary power-law fractal random field. On the other hand, in Section 3, we have demonstrated the consistency, efficiency, and low variance of appropriate MWE methods for simulating stationary fractal random fields. These methods have been developed recently by two of the authors[9, 10, 13] and are being applied elsewhere to problems in turbulent diffusion with fractal fields.[9, 11]

ACKNOWLEDGMENTS

A. J. M. is partially supported by grants NSF DMS 99301094, ARPA N00014-92-J-1796, ONR N00014-89-J-1044.P00003, and ARO DAAL03-92-G-0010. F. W. E. is supported by ARPA N00014-92-J-1796. D. J. H. was a graduate student at PACM at Princeton University supported by grants ARO DAAL03-92-G-0010 and ARO AASERT DAAH04-93-G-0341. R. M. M. is an NSF postdoctoral fellow supported by grant NSF DMS 9407547.

REFERENCES

1. M. Lesieur, *Trubulence in Fluids* (Kluwer, Boston, 1990), Chapter 8, and references therein.
2. W. McComb, *The Physics of Fluid Turbulence* (Clarendon Press, Oxford, 1990), Chapters 12 and 13, and references therein.
3. G. Csanady, *Turbulent Diffusion in the Environment* (Reidel, Dordrecht, Holland, 1973).
4. G. Dagan, Theory of solute transport by ground water, *Annu. Rev. Fluid Mech.* **19**:183–215 (1987).
5. F. Williams, Turbulent combustion, in *The Mathematics of Combustion*, J. Buckmaster, ed. (SIAM, Philadelphia, 1985), pp. 97–131.
6. J. Feder, *Fractals* (Plenum Press, New York, 1988), Chapters 9–14.

7. R. F. Voss, Random fractal forgeries, in *Fundamental Algorithms in Computer Graphics*, R. A. Earnshaw, ed. (Springer-Verlag, Berlin), pp. 805–835.
8. J. Viecelli and E. Canfield, Functional representation of power-law random fields and time series, *J. Comp. Phys.* **95**:29–39 (1991).
9. F. Elliott and A. Majda, A wavelet Monte Carlo method for turbulent diffusion with many spatial scales, *J. Comp. Phys.* **113**:82–109 (1994).
10. F. Elliott and A. Majda, A new algorithm with plane waves and wavelets for random velocity fields with many spatial scales, *J. Comp. Phys.* **117**:146–162 (1995).
11. F. Elliott and A. Majda, Monte Carlo simulation of pair dispersion over an inertial range with many decades, *Phys. Fluids* (1995), submitted.
12. B. Alpert, Sparse representation of smooth linear operators, Ph.D. thesis, Department of Computer Science, Yale University (December 1990).
13. F. Elliott and A. Majda, The convergence of multi-wavelet Monte Carlo methods for fractal random fields, in preparation.
14. J. Eggers and S. Grossman, Effect of dissipation fluctuations on anomalous velocity scaling in turbulence, *Phys. Rev. A* **45**:2360–2369 (1992).
15. A. Juneja, D. Lathrop, K. Sreenivasan, and G. Stolovitzky, Synthetic turbulence, *Phys. Rev. E* **49**:5179–5194 (1994).
16. R. Benzi, L. Biferale, A. Crisanti, G. Paladin, M. Vergassola, and A. Vulpiani, A random process for the construction of multiaffine fields, *Physica D* **65**:352–358 (1993).